

A High-Efficiency and High-Accuracy Polarimeter for Solar Magnetic Field Measurements

Deqing Ren¹ • Zijian Han^{2,3,4} • Jing Guo^{2,3}

Received: 20 December 2019 / Accepted: 24 July 2020

© Springer Nature B.V. 2020

Abstract Solar activity is dominated by the magnetic field. Nowadays, a polarimeter is a mandatory tool to measure solar magnetic fields, which are generally faint and correspond to a polarization of an order of 10^{-2} – 10^{-4} . As such, polarization measurements of high efficiency with a high accuracy are crucial to investigate faint magnetic fields. Here we propose a high-efficiency and high-accuracy polarimeter, which is based on a pair of nematic liquid crystal variable retarders (LCVRs) and a Wollaston prism (WP). It uses a dedicated Stokes modulation strategy to achieve high efficiency. A calibration unit (CU) is developed to measure the polarimeter response matrix, which provides a high-precision calibration to correct possible systematic errors. Compared with other traditional polarimeters, the modulation scheme of our polarimeter is flexible. In addition to be able to measure all the three Stokes polarization components (Q, U, or V) simultaneously, it can also measure one or two of these polarization components alone, with high polarization efficiency. Dedicated alignment and calibration techniques optimized for our polarimeter are developed and high measurement accuracy is achieved. In our laboratory experimental test, our two-image based polarization measurement delivers an overall measurement accuracy of the order of 10⁻⁴, which is about 10 times better, compared with our previous polarimeters that use the traditional four-image polarization modulation. This work provides a new option for high-efficiency and high-accuracy polarization measurement for future solar synoptic observations.

D. Ren ren.deqing@csun.eduZ. Han zjhan@niaot.ac.cnJ. Guo

jguo@niaot.ac.cn

Published online: 06 August 2020

Physics & Astronomy Department, California State University Northridge, Northridge 91330, USA

- National Astronomical Observatories/Nanjing Institute of Astronomical Optics & Technology, Chinese Academy of Sciences, Nanjing 210042, China
- ³ Key Laboratory of Astronomical Optics & Technology, Nanjing Institute of Astronomical Optics & Technology, Chinese Academy of Sciences, Nanjing 210042, China
- ⁴ University of Chinese Academy of Sciences, Beijing 100049, China



109 Page 2 of 23 D. Ren et al.

Keywords Instrumentation and data management \cdot Polarization \cdot Optical \cdot Magnetic fields \cdot Chromosphere

1. Introduction

Measurements of solar magnetic fields help us to explore and research the intrinsic properties of the solar atmosphere (Hofmann and Rendtel, 2003). Polarimetry measurements are routinely used to infer the solar magnetic fields through the Zeeman and Hanle effects (Hough, 2005; Asensio Ramos, Trujillo Bueno, and Landi Degl'Innocenti, 2008). With the access to large solar telescopes, polarization signals related with electromagnetic radiation are being measured with the highest possible resolution and accuracy, finding clues to characterize atmospheric parameters in different structures, from the fine structure of the quiet Sun to the largest sunspots (Beck et al., 2005; Solanki, Inhester, and Schüssler, 2006). As such, polarimetric instruments have been equipped within the major solar telescopes, such as the Advanced Solar Polarimeter (ASP: Skumanich et al., 1997), the Polarimetric Littrow Spectrograph (POLIS: Beck et al., 2005), the Spectro-Polarimeter for Infrared and Optical Regions (SPINOR: Socas-Navarro et al., 2006), and the Polarization Analyzer at 1-m New Vacuum Solar Telescope (NVST: Liu et al., 2014). Among them, the mechanical modulation strategy is employed, which achieves different modulation states by rotating waveplates. However, the rotatable mechanics limits the modulation speed, and also typically renders the image wandering on the focal plane (Wolfe and Chipman, 2006). Both shortcomings are the source of uncertainties, decreasing the accuracy in the modulation and polarization reconstruction. Alternatively, one can use a pair of liquid crystal variable retarders (LCVRs) to achieve the so-called solid-state modulation without the use of any mechanical device. An LCVR is an electro-optical modulator which achieves phase retardance variation by applying a corresponding voltage. A great merit of using an LCVR is the capability to achieve a moderate modulation speed, typically in tens of milliseconds, without any physical movement (Zangrilli et al., 2003; Shih, Hsieh, and Chao, 2014). In addition, it is able to eliminate the image wandering phenomenon. Therefore, some advanced solar polarimeters frequently employ the solid-state liquid crystal modulators, for example, the Flare Genesis Mission (FGM: Bernasconi et al., 2000), the Vector-Spectromagnetograph (VSM) of the Synoptic Optical Long-term Investigations of the Sun (SOLIS) instrument suite at the National Solar Observatory (NSO: Keller, Harvey, and Giampapa, 2003), the LC polarimeter for eclipse observations of the K-corona (EKPol: Zangrilli et al., 2006), the Facility Infrared Spectropolarimeter (FIRS) installed at the Dunn Solar Telescope (DST: Jaeggli et al., 2010), the Visible Imaging Polarimeter (VIP) operated at the German Vacuum Tower Telescope (Beck et al., 2010), the High-resolution Visible and Infrared Spectrograph (HiVIS) polarimeter on the 3.67 m Advanced Electro-Optical System telescope (AEOS: Harrington et al., 2010), the Imaging Magnetograph eXperiment (IMaX: Martínez Pillet et al., 2011), the Highsensitivity and High-accuracy Polarimeter (HHP: Guo et al., 2017), and the Polarimetric and Helioseismic Imager on the Solar Orbiter (SO/PHI: Parejo et al., 2019).

A modulation scheme is important for the design of a polarimeter, since it is closely related to the polarization measurement efficiency and the measurement accuracy. Some polarimeters use a Stokes-balanced modulation scheme, which equalizes uncertainties and maximizes the signal-to-noise (SNR) of the acquired images (Tyo, 2002; Asensio Ramos and Collados, 2008). However, for a single image, all the Stokes components contribute to the light intensity signal, which easily brings about potential crosstalk among the Stokes



components (Barrick, Benedict, and Sabin, 2010). A direct method is to reduce the simultaneous contribution of all Stokes components in each image, so that only one polarization component would contribute to the modulated intensity signal (Horn and Hofmann, 1999; Casini, de Wijn, and Judge, 2012). Meanwhile, using a polarizing beam splitter, the dual-beam polarimetry can effectively eliminate the crosstalk of $I \rightarrow Q$, U, V (Hou, de Wijn, and Tomczyk, 2013). The use of a calibration unit (CU) can quantify the system response matrix of a polarimeter, providing a numerical correction of the crosstalk or systematic error (Beck et al., 2005; Hofmann, 2007; Bettonvil et al., 2010). These characteristics can also allow for high accuracy in polarimetric measurements.

In this article, we propose a high-efficiency and high-accuracy polarimeter based on a pair of LCVRs and a Wollaston prism (WP) for our solar synoptic observations, in which high polarization efficiency and high accuracy are the top priorities. Our polarimeter uses a dedicated modulation strategy to maximize the polarization efficiency for the differential polarization measurements. As such, our polarimeter has several advantages. Firstly, in addition to measure all the Stokes components simultaneously as the traditional polarimeters that use four images for the modulation, our polarimeter is able to measure each Stokes component individually with minimum image number requirement in the modulation, with highest efficiency. On the other hand, depending on the nature of the scientific questions, only one or two polarization components may need to be measured. For example, to retrieve the prominence magnetic fields using both spectral lines of helium D3 and $H\alpha$, only the two Q and U linear polarization components were used (Bommier, Sahal-Brechot, and Leroy, 1981; Bommier et al., 1994; Leroy, Bommier, and Sahal-Brechot, 1983, 1984). The SOLIS Vector Spectromagnetograph only measures one circular polarization component V in the CaII 854.2 nm spectral line, since the other two polarization components are too weak to be measured (Keller, Harvey, and Giampapa, 2003). To derive the system response matrix and to allow for the on-site calibration to correct potential systematic errors, we developed a compact CU for this polarimeter. The above characteristics allow our polarimeter to achieve a high efficiency and a high accuracy. The remaining of this article is arranged as follows. In Section 2, we introduce our polarimeter design philosophy, including the optical setup and dedicated modulation strategy. Section 3 presents the alignment and calibration methodologies. Experimental results and discussion are provided in Section 4. In Section 5, we summarize our conclusions for this work.

2. The Proposed High-Efficiency and High-Accuracy Polarimeter

2.1. System Setup

For solar synoptic observations, our polarimeter can be used with a dedicated telescope that consists of transmission optics lenses, as those used for the synoptic observations at the Kodaikanal Observatory (Ravindra et al., 2016). Such a transmission telescope should have a negligible induced instrumental polarization over a large field of view. A standard commercial Cassegrain telescope such as the Celestron EdgeHD 14" Optical Tube Assembly can also be used. Because of the symmetry, this telescope should have an induced polarization less than 10⁻⁴ for wide field imaging (Sen and Kakati, 1997). For a large telescope with a Coudé focus, it is possible to be free of induced instrumental polarization by using a single retarding plate (Martinez Pillet and Sanchez Almeida, 1991). Solar synoptical telescopes typically have an optical aperture size between 200–400 mm (Keller, Harvey, and Giampapa, 2003; Ravindra et al., 2016). The polarimeter and tunable Lyot filter (if used)



109 Page 4 of 23 D. Ren et al.

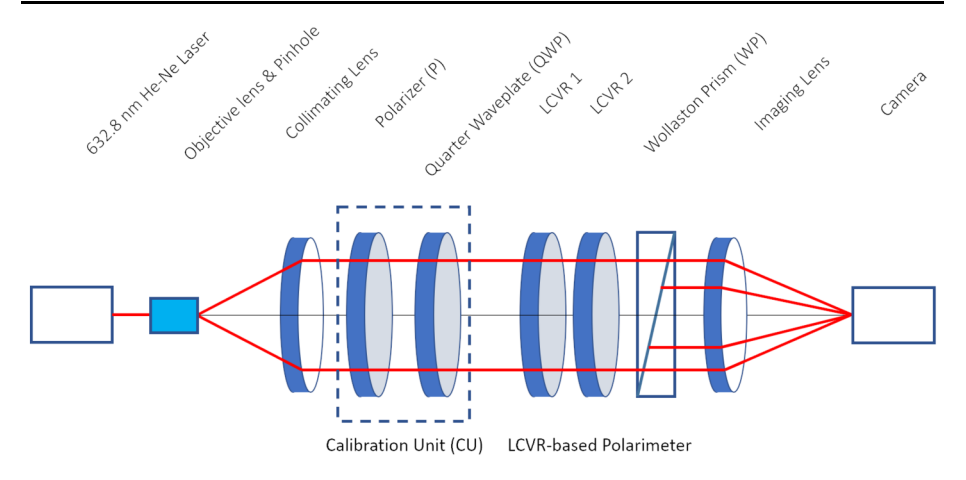


Figure 1 Schematic diagram of the proposed high-efficiency polarimeter.

can be installed immediately after the telescope focus. In such a way, the polarimetry measurement accuracy of the system will be determined by the polarimeter only. The schematic diagram of the proposed high-efficiency polarimeter is shown in Figure 1. In the laboratory experiment, a point source is used, which is generated by an assembly consisting of a 632.8 nm He–Ne laser, a microscope objective lens and a pinhole. The light beam from the collimating lens then goes through the polarimeter calibration unit, which is composed of a linear polarizer (P) with an extinct ratio of approximately 100,000: 1 and a rotating quarter-wave plate (QWP) defined at the 633 nm wavelength. The azimuth angle of the linear polarizer is fixed, while the QWP is mounted on a Thorlabs motorized rotational mount and its fast-axis can be rotated accordingly with an absolute angular position accuracy of $\pm 0.014^{\circ}$. The CU is only needed to switch into the polarimeter optical path during the polarization calibration as shown in Figure 1. During the polarization measurement, it will not be a part of the polarimeter. The core modulation elements for the proposed polarimeter are two liquid crystal variable retarders (LCVR 1 and LCVR 2) and a Wollaston prism. The nematic LCVRs, manufactured by Thorlabs, are antireflective coated in 350-750 nm wavelength range, without compensation for the 0° retardance. Each LCVR is operated through a separate Thorlabs LCC25 controller, which provides a 0-25 VAC voltage with 0.001 V resolution. A Thorlabs WPQ10 Wollaston prism is used as the polarization beam splitter in the downstream of the optical path, which separates the light into two orthogonally polarized beams with a small separation angle, with a typical value of 1° in our system. The Wollaston prism delivers a high extinction ratio on the order of 100, 000: 1. The two beams are recorded by a Photometrics Prime 95B scientific CMOS (sCMOS) camera with a low readout noise on the order of 2 e^- and a 16-bit high-dynamic range. Dedicated LabVIEW codes are developed to control the two LCVRs and the sCMOS camera.

2.2. Polarization Modulation and Demodulation

As shown in Figure 1, for the polarimeter system excluding the calibration unit, the relationship between the input Stokes vector $S_{in} = (I, Q, U, V)^T$ and output Stokes vector $S_{out} = (I', Q', U', V')^T$ can be calculated via the so-called Mueller matrices,

$$S_{out} = M_{WP} \cdot M_{LCVR2} \cdot M_{LCVR1} \cdot S_{in}, \tag{1}$$



where M_i stands for the Mueller matrix of the optical element i. Assuming that the light beam propagates along the Z-axis in the right-handed Cartesian coordinate system. Let us define the X-axis in the same direction as that of the Q Stokes component. A general Mueller matrix of a Wollaston prism with a transmission axis angle of β to the X direction is given by

$$M_{WP}(\beta) = \frac{1}{2} \begin{pmatrix} 1 & \cos 2\beta & \sin 2\beta & 0\\ \cos 2\beta & \cos^2 2\beta & \cos 2\beta \sin 2\beta & 0\\ \sin 2\beta & \cos 2\beta \sin 2\beta & \sin^2 2\beta & 0\\ 0 & 0 & 0 & 0 \end{pmatrix}, \tag{2}$$

where $\beta = 0^{\circ}$ or 90° for our polarimeter, which means that the two transmission axes of the Wollaston prism are defined in the X and Y direction, respectively.

The fast axis angles of LCVRs 1 and 2 with respect to the X direction are 22.5° and 45°, respectively. For each LCVR with a phase retardation ϕ , its Mueller matrix is given by

$$M_{LCVR1}(\alpha_1 = 22.5^{\circ}, \phi_1) = \frac{1}{2} \begin{pmatrix} 2 & 0 & 0 & 0 \\ 0 & 1 + \cos\phi_1 & 1 - \cos\phi_1 & -\sqrt{2}\sin\phi_1 \\ 0 & 1 - \cos\phi_1 & 1 + \cos\phi_1 & \sqrt{2}\sin\phi_1 \\ 0 & \sqrt{2}\sin\phi_1 & -\sqrt{2}\sin\phi_1 & 2\cos\phi_1 \end{pmatrix}, \quad (3)$$

$$M_{LCVR2}(\alpha_2 = 45^\circ, \phi_2) = \begin{pmatrix} 1 & 0 & 0 & 0\\ 0 & \cos\phi_2 & 0 & -\sin\phi_2\\ 0 & 0 & 1 & 0\\ 0 & \sin\phi_2 & 0 & \cos\phi_2 \end{pmatrix}. \tag{4}$$

Based on the above equations, different modulation status with different retardance combinations (ϕ_1, ϕ_2) can be achieved. The light incident on the polarimeter can be modulated as a dual-beam intensity signal, and recorded by a camera. Note that the intensities of two light beams are expressed as $I_L(\phi_1, \phi_2)$ and $I_R(\phi_1, \phi_2)$, respectively.

By carefully analyzing the above equations, we found that the following combinations can be used to measure each Stokes polarization component with the maximum efficiency:

i) To measure the linearly polarized Q component, the LCVR 1 retardance is fixed at 0° , while the LCVR 2 retardance is switched between 0° and 180° , respectively. The normalized Q component is solved as

$$\frac{Q}{I} = \frac{1}{2} \left[\frac{I_L(0^\circ, 0^\circ) - I_L(0^\circ, 180^\circ)}{I_L(0^\circ, 0^\circ) + I_L(0^\circ, 180^\circ)} - \frac{I_R(0^\circ, 0^\circ) - I_R(0^\circ, 180^\circ)}{I_R(0^\circ, 0^\circ) + I_R(0^\circ, 180^\circ)} \right]. \tag{5}$$

ii) To measure the linearly polarized U component, the LCVR 1 retardance is fixed at 180° , while the LCVR 2 retardance is switched between 0° and 180° , respectively. The normalized U component is solved as

$$\frac{U}{I} = \frac{1}{2} \left[\frac{I_L(180^\circ, 0^\circ) - I_L(180^\circ, 180^\circ)}{I_L(180^\circ, 0^\circ) + I_L(180^\circ, 180^\circ)} - \frac{I_R(180^\circ, 0^\circ) - I_R(180^\circ, 180^\circ)}{I_R(180^\circ, 0^\circ) + I_R(180^\circ, 180^\circ)} \right].$$
(6)

iii) To measure the circularly polarized V component, the LCVR 1 retardance is fixed at 0° , while the LCVR 2 retardance is switched between 90° and -90° , respectively. The



Table 1 Modulation status and LCVR retardance combinations.

No	Modulation status	LCVR 1 retardance	LCVR 2 retardance
1	$I\pm Q$	0	0
2	$I \mp Q$	0	$\lambda/2$
3	$I\pm U$	$\lambda/2$	0
4	$I \mp U$	$\lambda/2$	$\lambda/2$
5	$I \pm V$	0	$\lambda/4$
6	$I \mp V$	0	$-\lambda/4$

normalized V component is solved as

$$\frac{V}{I} = \frac{1}{2} \left[\frac{I_L(0^\circ, 90^\circ) - I_L(0^\circ, -90^\circ)}{I_L(0^\circ, 90^\circ) + I_L(0^\circ, -90^\circ)} - \frac{I_R(0^\circ, 90^\circ) - I_R(0^\circ, -90^\circ)}{I_R(0^\circ, 90^\circ) + I_R(0^\circ, -90^\circ)} \right]. \tag{7}$$

By changing the phase retardance combinations of the two LCVRs according to the above equations, the polarization signal can be modulated and the associated Stokes component can be derived accordingly via the so-called demodulation. Table 1 summarizes the modulation strategy and its corresponding Stokes polarization component that can be measured. In the modulation status column, the signs + and - stand for the left and right beam, respectively. Here, in our polarization modulation, it is clear that each time two images can be directly used to derive one Stokes component, which maximizes the polarization measurement efficiency of the corresponding Stokes component; this will be discussed in detail in the next subsection. In addition, since only one Stokes component is measured in these two associated images, it has the potential to avoid the crosstalk between the four Stokes components.

2.3. Polarization Efficiency

Polarization measurement efficiency is a critical parameter for a polarimeter development, since a high efficiency is an indication of a high signal-to-noise ratio, which eventually determines the uncertainties to derive the corresponding Stokes components (Collados, 1999; del Toro Iniesta and Collados, 2000). The dedicated modulation configuration of our polarimeter provides the flexibility to measure each polarization component individually and thus maximizes the corresponding measurement efficiency. This is important for the polarization measurements, as in many observations only one or part of the Stokes components need to be measured. However, the conventional polarimeters use at least four modulation images simultaneously to measure the four Stokes polarization components which easily leads to crosstalks between different Stokes components. The crosstalk between the polarization components may contaminate the measurement purity and thus reduce the polarization measurement accuracy. Based on our polarimeter, we discuss different configurations for the measurement of the Stokes components, which could be used.

i) Measurements of Q and U components simultaneously

For a solar polarimeter to measure the weak magnetic field, a maximum overall polarization efficiency of 1 is desirable. The optimization of the modulation configuration for the maximum efficiency consists of minimizing the uncertainty for each of the Stokes-component measurements. As shown in Table 1, when the four images from number 1 to number 4 are used, two linearly polarized components Q and U of the input light can be measured. According to the Mueller calculus, for the four intensity images I =



 $(I_1, I_2, I_3, I_4)^T$, the associated input Stokes components can be solved from the equation $I = M \cdot S_{in}$, where M is the modulation matrix of the polarimeter. The demodulation matrix of a polarimeter is $D = (M^T M)^{-1} M^T$; this is the pseudoinverse matrix of M. For the proposed 2-beam system, from Equations 5 and 6, we have

$$M = \begin{pmatrix} 1 & 1 & 0 & - \\ 1 & -1 & 0 & - \\ 1 & 0 & 1 & - \\ 1 & 0 & -1 & - \end{pmatrix}, \text{ thus } D = \begin{pmatrix} 0.25 & 0.25 & 0.25 & 0.25 \\ 0.5 & -0.5 & 0 & 0 \\ 0 & 0 & 0.5 & -0.5 \\ - & - & - & - \end{pmatrix}.$$
(8)

Assuming that $(\epsilon_I, \epsilon_Q, \epsilon_U, \epsilon_V)$ are the polarization efficiencies of the Stokes components (I, Q, U, V). The polarization efficiency of a 4-image system can be calculated as (del Toro Iniesta and Collados, 2000)

$$\epsilon_i = \left(n\sum_{j=1}^n D_{ji}^2\right)^{-\frac{1}{2}},\tag{9}$$

where n = 4 is the total image number. i = 1, 2, 3, and 4 stands for any of the corresponding four Stokes components. This yields the efficiency for each polarization component as

$$\left(\epsilon_{I}, \epsilon_{Q}, \epsilon_{U}, \epsilon_{V}\right) = \left(1, \frac{\sqrt{2}}{2}, \frac{\sqrt{2}}{2}, 0\right). \tag{10}$$

It should be noted that the intensity efficiency ϵ_I is always equal to 1 for the 2-beam system. The modulation configuration delivers the same polarization efficiency for each of the Q and U components, and achieves the highest overall polarization efficiency of 1, i.e.

$$\sqrt{\epsilon_Q^2 + \epsilon_U^2 + \epsilon_V^2} = 1.0. \tag{11}$$

ii) Measurement of the V component only.

In a similar modulation to the previous case, the V component can be measured, but only using two images, numbers 5 and 6, listed in Table 1. In this case, since the observation time is doubled because only two images are needed, compared with the previous case that needs four images, the V component has a measurement efficiency of 100% in real scientific observations. Thus, the polarization efficiency is

$$\left(\epsilon_{I}, \epsilon_{Q}, \epsilon_{U}, \epsilon_{V}\right) = \left(1, 0, 0, 1\right). \tag{12}$$

In this case, the configuration delivers the highest polarization efficiency for the circular polarization component V.

iii) Measurements of Q, U, and V simultaneously.

The three components Q, U, and V can be measured using all the six images from number 1 to number 6, shown in Table 1, and the polarization efficiency of the three components are

$$\left(\epsilon_{I}, \epsilon_{Q}, \epsilon_{U}, \epsilon_{V}\right) = \left(1, \frac{\sqrt{3}}{3}, \frac{\sqrt{3}}{3}, \frac{\sqrt{3}}{3}\right). \tag{13}$$

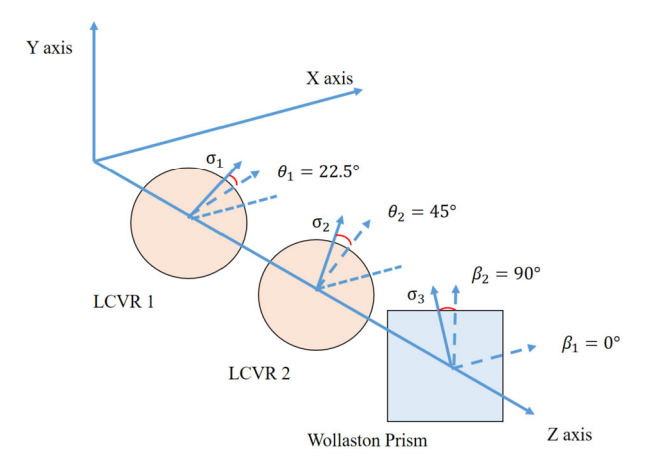
Accordingly, the overall efficiency is

$$\sqrt{\epsilon_Q^2 + \epsilon_U^2 + \epsilon_V^2} = 1.0. \tag{14}$$



109 Page 8 of 23 D. Ren et al.

Figure 2 Polarization elements and their associated azimuth errors



It is clear that our polarimeter can use different configurations to measure different Stokes components. When only one of the polarization components is measured, it delivers a maximum efficiency of 1.0.

3. System Calibrations

For a polarimeter, the alignment of the modulation elements is a critical step to achieve a high accuracy. If any parameter value of an element seriously differs from the theoretical estimation, one would not be able to derive the polarization component correctly. In addition, the calibration of the instrumental polarization is also an important step to quantify the crosstalk, and provides a means to correct a possible system alignment error (if there is) by finding the polarimeter response matrix.

3.1. Alignment Error Sensitivity Analysis

The alignment error analysis considers the azimuth error of the polarization optics. For the proposed polarimeter, the X and Y directions are defined in advance in the Cartesian coordinate system. Under the circumstance of a point light source, if the two spots exiting the Wollaston prism distribute horizontally, the reference $\pm X$ axis is defined.

For the error of the fast axis azimuth, both LCVRs and Wollaston prism would be taken into consideration. Figure 2 illustrates the relationships of possible error sources in the polarization optics, which includes the azimuth errors of the two LCVRs and the Wollaston prism, expressed as σ_1 , σ_2 , and σ_3 , respectively.

From Table 1, if all I, Q, U, and V components are included, the modulation matrix of the system is

$$M = \begin{pmatrix} 1 & 1 & 0 & 0 \\ 1 & -1 & 0 & 0 \\ 1 & 0 & 1 & 0 \\ 1 & 0 & -1 & 0 \\ 1 & 0 & 0 & 1 \\ 1 & 0 & 0 & -1 \end{pmatrix},\tag{15}$$

so that the six intensity images $I_0 = (I_1, I_2, I_3, I_4, I_5, I_6)^T$ and the input Stokes vector $S_{in} = (I, Q, U, V)^T$ are connected with the modulation matrix as $I_0 = M \cdot S_{in}$. In the remaining



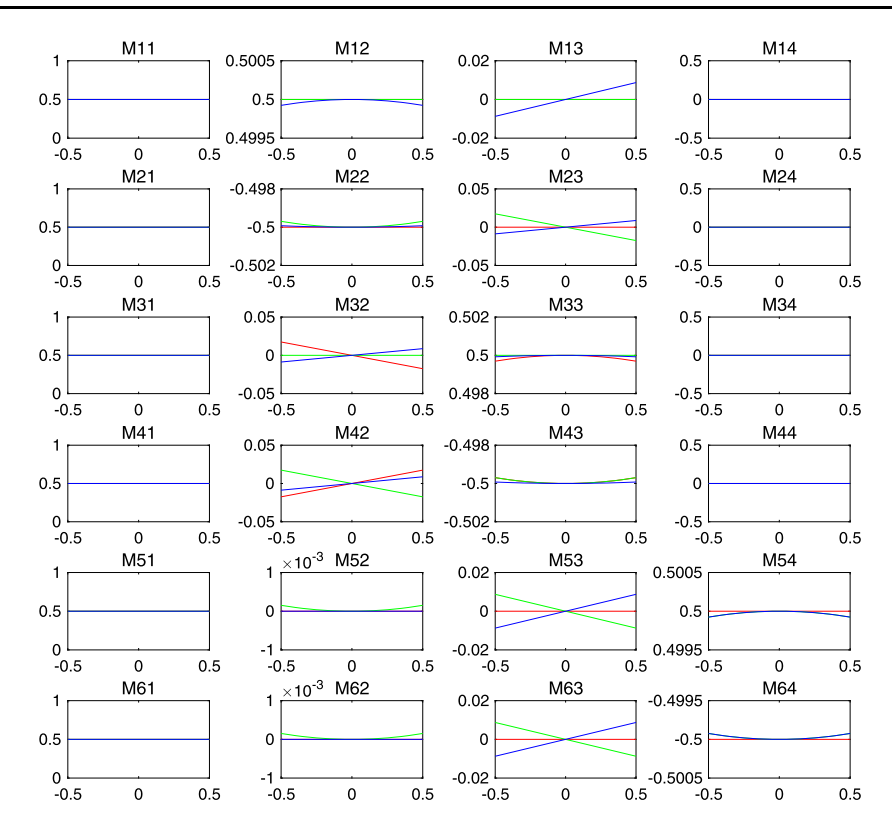


Figure 3 Influence on the modulation matrix from the azimuthal errors σ_1 , σ_2 , and σ_3 for one beam light output case only. The X coordinate is the azimuth error in degrees. The Y coordinate is the value of the elements in the systematic Mueller matrix. Red, green, and blue lines are azimuth from σ_1 , σ_2 , and σ_3 , respectively.

part of this article, this 6×4 -element modulation matrix M will be used to characterize our polarimeter.

We conduct a sensitivity analysis with each of the σ_1 , σ_2 , and σ_3 , respectively. In the numerical simulation, the impact on the systematic Mueller matrix is considered under the axis azimuth errors σ_1 , σ_2 , and σ_3 , respectively, with a range from -0.5° to 0.5° individually. This range is consistent with that of the rotational mounts currently adopted in this experimental system. Figure 3 illustrates the impact to the 6×4 modulation matrix of the system caused by σ_1 , σ_2 , and σ_3 , respectively. Each sub-figure shows the value of the corresponding element in the matrix in Equation 15. The red, green, and blue curves represent the shift result from the azimuth errors of σ_1 , σ_2 , and σ_3 , respectively.

Based on the modulation matrix, we can calculate the measurement accuracy for each Stokes component as a function of these errors. From Figure 3, it is obvious that the misalignment of fast axes mainly introduces the crosstalk between Q and U components, and the numerical results are shown in the elements M_{13} , M_{23} , M_{32} , M_{42} , M_{53} , M_{63} . If the polarimeter needs an accuracy of 5×10^{-3} level, the azimuth error should be $\sigma < \pm 0.235^{\circ}$. If the polarimeter needs an accuracy level of 2×10^{-3} , the azimuth error should be $\sigma < \pm 0.115^{\circ}$.



109 Page 10 of 23 D. Ren et al.

3.2. LCVR Retardance Measurements

The polarization modulation is performed by the two LCVRs, in which the required phase retardance is controlled by applying a voltage to the corresponding LCVR. An accurate retardance-voltage relationship is needed to operate an LCVR properly. The retardance is measured via the light intensity variation when the testing LCVR is sandwiched between two perpendicular or parallel linear polarizers (Wu, Efron, and Hess, 1984). The fast axis of the testing LCVR is at 45° from either axis of the polarizer. For our proposed polarimeter, the LCVR is sandwiched between a fixed polarizer and a WP, so as to measure the light intensities L_{\perp} and L_{\parallel} exiting WP simultaneously. The transmitted intensity and the LCVR retardance relationships are given by

$$L_{\perp} = I_0 \exp(-\alpha_0 d) \sin^2 \frac{\delta}{2},\tag{16}$$

$$L_{\parallel} = I_0 \exp(-\alpha_0 d) \cos^2 \frac{\delta}{2},\tag{17}$$

where α_0 represents the liquid crystal absorption coefficient for the ordinary ray, and d is the thickness of the liquid crystal. The retardance can be derived from the ratio of L_{\perp} and L_{\parallel} , which is

$$|\delta| = \begin{cases} N\pi + 2 \tan^{-1} \sqrt{\frac{L_{\perp}}{L_{\parallel}}} & N = 0, 2, 4, \dots, \\ (N+1)\pi - 2 \tan^{-1} \sqrt{\frac{L_{\perp}}{L_{\parallel}}} & N = 1, 3, 5, \dots, \end{cases}$$
(18)

where $N\pi$ is the ambiguity for the determination of δ , which is determined by the characteristics of the liquid crystal.

Figure 4 shows the test results of the applied voltage and retardance for the two LCVRs, respectively. Table 2 shows the calibrated voltages required by the modulation scheme in our polarimeter. In the calibration, the voltages for the two LCVRs are shifted from 0.00 V to 6.00 V with an interval of 0.01 V. The room temperature was 27.6 °C during the calibrations.

Since the LCVRs are not compensated for a 0° phase retardance, some of the desired retardances will add 360° when used for our polarimeter. For example, 0° will be replaced by 360°, and -90° will be replaced by 270°. Please note that adding 360° will not change the modulation matrix.

3.3. Instrumental Polarization Calibration

A polarimeter actual measurement accuracy in observations depends critically on its calibration. This calibration can be done by placing the calibration unit in the front of the polarimeter. This cannot be perfect for any polarimeter and some alignment errors may exist, which may reduce the polarization accuracy. Considering a polarimeter, the true input Stokes vector S_{true} and the measured Stokes vector S_m are related by a 4 × 4-element polarimeter response matrix X as $S_m = X \cdot S_{true}$.

The accurate determination of the polarimeter response matrix X is the goal of the polarimeter calibration, which can be achieved using a series of known input Stokes vectors generated by the CU, and then measuring the associated polarimeter output Stokes vectors. The data can then be used to solve the polarimeter response matrix X. As illustrated in Figure 1, the proposed polarimeter uses a CU for the modulation matrix calibration. The CU includes a fixed linear polarizer with its fast axis at 0° , and a rotating QWP mounted on a



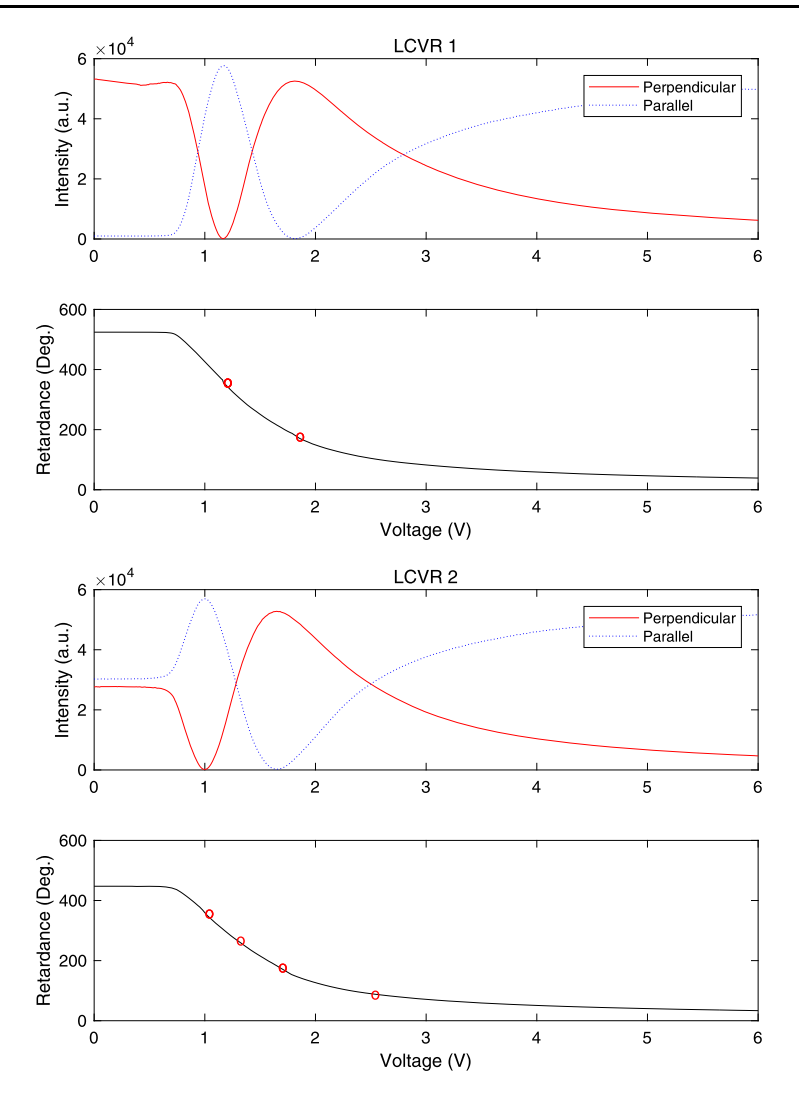


Figure 4 The calibrated retardance-voltage relationships of LCVRs 1 and 2. Upper panel: LCVR 1. Lower panel: LCVR 2. For each LCVR, we show both the intensity and the retardance curves.

Table 2 Calibrated voltages for LCVRs 1 and 2 in the modulation scheme.

No	Modulation status	LCVR 1		LCVR 2	
		Retardance	Voltage	Retardance	Voltage
1	$I \pm Q$	0°	1.165 V	0°	0.995 V
2	$I \mp Q$	0°	1.165 V	180°	1.663 V
3	$I\pm U$	180°	1.819 V	00	0.995 V
4	$I \mp U$	180°	1.819 V	180°	1.663 V
5	$I \pm V$	0°	1.165 V	-90°	1.283 V
6	$I \mp V$	0°	1.165 V	90°	2.499 V



109 Page 12 of 23 D. Ren et al.

step motor rotational stage. The CU generates discrete known polarization states to calibrate the system and thus derive the polarimeter response matrix X, which can be used to correct potential system errors. The CU generated Stokes vectors $S_{true} = S_{CU}$ and measured output Stokes vectors S_m on the polarimeter are connected by the 4 × 4-element polarimeter response matrix X as

$$S_m = X \cdot S_{CU}. \tag{19}$$

For a CU consisting of a linear polarizer and a QWP, the CU generated Stokes vector S_{CU} can be calculated as

$$S_{CU} = M_{OWP}(\theta_i) \cdot M_P(\theta_P) \cdot S, \tag{20}$$

where M_{QWP} and M_P denote the Mueller matrices of the QWP and of the linear polarizer in the CU, respectively, $\theta_i = (5i)^\circ$ and $\theta_P = 0^\circ$ are the azimuth angle of the fast axis of the QWP and transmission axis of the polarizer, respectively. i = 0, 1, ..., 36 is the rotational angular count number of the QWP. In our test, we use a non-polarized light source, and therefore $S = (I, 0, 0, 0)^T$ is the non-polarized incident light on the CU with an averaged intensity I. In the calibration, supposing that the QWP rotation angle θ_i is between 0° and 180° with a 5° -step, the CU generated Stokes vectors are

$$S_{CU} = \frac{I}{2} \left(1, \cos^2 \theta_i, \sin 2\theta_i \cos 2\theta_i, \sin 2\theta_i \right)^T.$$
 (21)

So far, we have the input Stokes vectors in a group of $S_{4\times37}$ and we can also measure the output Stokes vectors of $S_{m,4\times37}$. The 4 × 4-element polarimeter response matrix, X, can be solved by using the singular value decomposition (SVD) inversion from Equation 19. For the proposed polarimeter, we found its polarimeter response matrix to be

$$X = \begin{pmatrix} 1.0000 & 0.0000 & 0.0000 & 0.0000 \\ -0.0543 & 1.0397 & -0.0201 & -0.0609 \\ -0.0035 & -0.0174 & 1.0183 & 0.0178 \\ -0.0013 & 0.0487 & -0.1058 & 0.9732 \end{pmatrix}.$$
(22)

The polarimeter response matrix can be combined with the modulation matrix defined by Equation 15 that includes all Stokes elements, and we define a calibrated modulation matrix M_{cal}

$$M_{cal} = M \cdot X = \begin{pmatrix} 0.9457 & 1.0397 & -0.0201 & -0.0609 \\ 1.0543 & -1.0397 & 0.0201 & 0.0609 \\ 0.9965 & -0.0174 & 1.0183 & 0.0178 \\ 1.0035 & 0.0174 & -1.0183 & -0.0178 \\ 0.9987 & 0.0487 & -0.1058 & 0.9732 \\ 1.0013 & -0.0487 & 0.1058 & -0.9732 \end{pmatrix},$$
(23)

so that the true input Stokes vector S_{true} can be derived from the 6-element measured intensity image vector I_0 with the calibrated modulation matrix as

$$S_{true} = (M_{cal})^{-1} \cdot I_0, (24)$$

where $(M_{cal})^{-1}$ is the pseudoinverse matrix of the M_{cal} , and can be obtained using the SVD approach. $I_0 = (I_1, I_2, I_3, I_4, I_5, I_6)^T$ is the image vector including the six measured intensity images listed in Table 1.



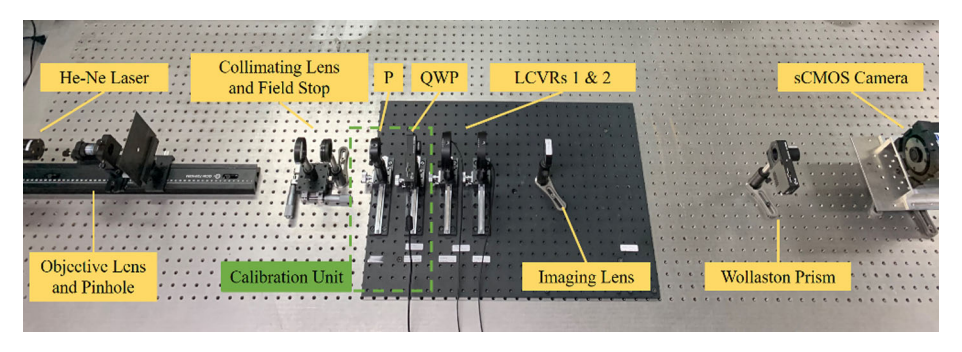


Figure 5 Photograph of the proposed polarimeter during a laboratory test.

4. Experimental Results and Discussion

4.1. Simultaneous Measurements of all Stokes Components for the Proposed Polarimeter

Figure 5 shows the photograph of our polarimeter during the laboratory test. In the experiment, we choose fully polarized light of different states to characterize and calibrate the system. As discussed previously, the polarimeter response matrix X from Equation 22 is used to correct the possible system errors. For each polarized light, all the six modulation states, which correspond to six intensity images $I_0 = \begin{pmatrix} I_1, I_2, I_3, I_4, I_5, I_6 \end{pmatrix}^T$, are driven by the LCVRs, and the light intensity signals are recorded by a scientific CMOS camera (Photometrics Prime 95B). All the acquired images are subtracted with dark-current images. For each modulation state, 100 intensity images are recorded and averaged as a master image to depress the light-source intensity variation, since the commercial He-Ne laser (Thorlabs HNL050R, with a working wavelength of 632.8 nm) we used as the light source typically has an intensity variation up to 5%. Since a point source is used for this test, a region-of-interest (ROI) with 25 × 25 pixels enclosing the point spread function (PSF) Airy disk is extracted for the performance characterization.

Figure 6 demonstrates the measured and calibrated results of 37 discrete states of the polarization light source Q, U, and V that will be used to test and calibrate our polarimeter. These are generated by a fixed linear polarizer and a rotating QWP, whose combination can generate any known polarization state and be used to calibrate our system. The fast axis of QWP rotates from 0° to 180° with an interval of 5°. Since any polarimeter may have some unavoidable residual error, as we discussed previously, the polarimeter response matrix X is used to calibrate our system. It can be seen that after the polarization calibration, the normalized Q, U, and V components are calibrated well following the theoretical values, even though there is some system error for each measured polarization signal before the calibration correction. Relative accuracy is measured after these calibrations. From Figure 6, it is clear that the input signal for each polarization component is variable and its value is determined by the rotation angle of the QWP. For example, the amplitude of the normalized Q varies between 0 and 1, with 1 as its maximum value. For each polarization component measurement, the input signal is aligned to make the amplitude (+ or - maximum value) of the measured polarization component (such as the U) to have a maximum value, since in this case it will have the best signal to noise ratio and thus facilitate high-accuracy measurements. Table 3 shows the root-mean-square (RMS) measurement error for each Stokes component,



109 Page 14 of 23 D. Ren et al.

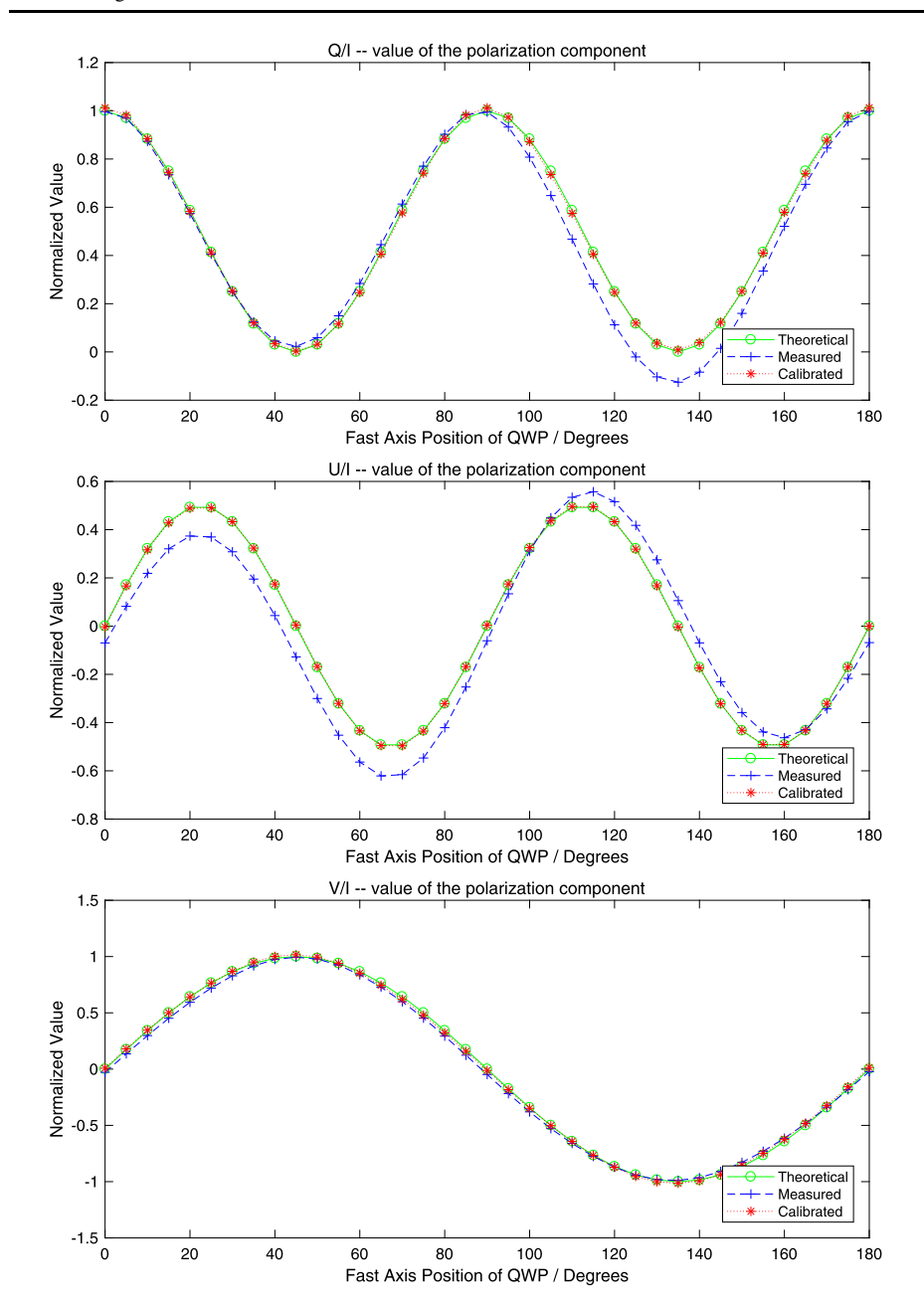


Figure 6 Measured and calibrated results of different generated states of polarized light. From top to bottom for the normalized Stokes Q, U, and V components, respectively. Green lines for theoretical data, blue lines for measured data before the polarization calibration, and red lines for data with polarization calibration.

which characterizes the relative accuracy of our polarimeter. The RMS error is defined as the standard deviation between measured and theoretical incident Stokes components. It includes the random photon noise, detector readout noise and all other possible noises. Here,



Table 3 Six-image modulation			
polarization accuracy	Normalized Stokes components	RMS error	
measurements.			
	(+)Q/I	2.905×10^{-4}	
	(-)Q/I	2.419×10^{-4}	
	(+)U/I	2.633×10^{-4}	
	(-)U/I	3.568×10^{-4}	
	(+)V/I	6.383×10^{-4}	
	(-)V/I	6.891×10^{-4}	

Table 4 Two-image modulation polarization accuracy measurements on V component only.

Normalized Stokes components	RMS error
(+)V/I (-)V/I	7.783×10^{-4} 8.826×10^{-4}

the symbols (+) and (-) indicate that the measurements are done at the maximum positive and maximum negative value of the associated input polarization signal, respectively. It can be seen that the proposed polarimeter achieves an accuracy of 7×10^{-4} for the circular polarization signal, and an accuracy around 3×10^{-4} for the linear polarization signal.

4.2. Partial Stokes-Component Measurements of the Proposed Polarimeter

In the previous subsection, the polarization accuracy of the proposed polarimeter is measured simultaneously on all of the three Stokes components Q, U and V. That is, the result is fully calibrated using all the six intensity images. As discussed previously, in many scientific observations, only partial components of the Stokes vector, such as V or Q and U, are needed to measure. In this subsection, we will discuss how to measure partial components of the Stokes vector.

i) Measurements of the V component only.

If only the circular polarization component V is required to be measured, only rows 5 and 6 in Equation 23 will be adopted for the demodulation, which corresponds to images numbers 5 and 6. Further, the coefficients for the two row polarization components Q and U should be rounded as 0. In this way, Q and U components will not be included in our calculation to derive V, and Equation 23 is now simplified as a 2×2 -component matrix, which only includes the elements from rows 5–6 and columns 1 and 2. Therefore, only two images are required for the measurement of the V component. As we will see, such a rounding off will almost not reduce our measurement accuracy. Table 4 shows the polarization accuracy of the V component, when only two images numbers 5 and 6 are used. It is obvious that the measurement accuracy of V in the two-image case is almost identical to that of the 6-image case discussed in the previous subsection.

ii) Measurements of the Q and U components simultaneously.

Similarly, if only the two linear polarization components Q and U are required to measure, rows 1 to 4 in Equation 23 will be adopted for the demodulation, corresponding to images 1 to 4. Furthermore, the V component coefficient should be rounded as 0, so that V will not be included in our calculation to derive the Q and U components. Now, Equation 23 is simplified as a 4×4 -component matrix, so that only four images are needed. Table 5 shows the polarization accuracy of Q and U components when using only the four images



109 Page 16 of 23 D. Ren et al.

Table 5 Four-image modulation polarization accuracy measurements on Q and U components only.

Normalized Stokes components	RMS error
(+)Q/I	3.241×10^{-4}
(-)Q/I	3.069×10^{-4}
(+)U/I	2.618×10^{-4}
(-)U/I	2.591×10^{-4}

1 to 4. Again, it is clear that the measurement accuracy of Q and U in the four-image case is almost identical to that of the 6-image case.

Comparing the results shown in Table 3, the polarization accuracy is almost on the same scale for both demodulation methods discussed in this subsection. It can be seen that the impact from the unmeasured Stokes component is negligible. Therefore, the proposed polarimeter can be used on real scientific observations for partial Stokes-component measurements. It is worth noting that our 2 or 4-image modulation can only be applied when other unmeasured polarization components have a smaller value than that of the measured one.

4.3. Results of the Traditional 4-Image Polarimeter

In order to compare our proposed modulation scheme with the traditional 4-image modulation one, we conducted an experiment under the same measurement conditions. The traditional 4-image modulation scheme we adopted here was previously used by the Imaging Magnetograph Experiment (IMaX: Martínez Pillet et al., 2011). It uses two LCVRs and the azimuth angles of the fast axes of the two LCVRs are 0° and 45° , respectively. The retardance combinations and corresponding voltages of the two LCVRs are listed in Table 6.

To compare the measurement result, we setup a polarimeter that uses the traditional modulation scheme with the IMaX. Considering one beam only, the modulation matrix of the IMaX is

$$M_{4-image} = \begin{pmatrix} 1 & \sqrt{3}/3 & \sqrt{3}/3 & \sqrt{3}/3 \\ 1 & \sqrt{3}/3 & -\sqrt{3}/3 & -\sqrt{3}/3 \\ 1 & -\sqrt{3}/3 & -\sqrt{3}/3 & \sqrt{3}/3 \\ 1 & -\sqrt{3}/3 & \sqrt{3}/3 & -\sqrt{3}/3 \end{pmatrix},$$
(25)

and its corresponding demodulation matrix is

$$D_{4-image} = \frac{1}{4} \begin{pmatrix} \frac{1}{\sqrt{3}} & \frac{1}{\sqrt{3}} & -\frac{1}{\sqrt{3}} & -\frac{1}{\sqrt{3}} \\ \frac{1}{\sqrt{3}} & -\sqrt{3} & -\sqrt{3} & \sqrt{3} \\ \frac{1}{\sqrt{3}} & -\sqrt{3} & \sqrt{3} & -\sqrt{3} \end{pmatrix}.$$
 (26)

In the ideal case, the efficiency of the polarization measurement $(\epsilon_I, \epsilon_Q, \epsilon_U, \epsilon_V)$ of the Stokes components (I, Q, U, V) is

$$\left(\epsilon_{I}, \epsilon_{Q}, \epsilon_{U}, \epsilon_{V}\right) = \left(1, \sqrt{3}/3, \sqrt{3}/3, \sqrt{3}/3\right). \tag{27}$$



Table 6 Resulting voltages for LCVRs 1 and 2 in the traditional 4-image modulation scheme.

No	LCVR 1		LCVR 2	
	Retardance	Voltage	Retardance	Voltage
1	315°	1.130 V	305.264°	1.546 V
2	315°	1.130 V	54.736°	3.743 V
3	225°	1.458 V	125.264°	2.013 V
4	225°	1.458 V	234.736°	1.417 V

Table 7 Traditional 4-image modulation scheme polarization accuracy measurements.

Normalized Stokes components	RMS noise value	
(+)Q/I	3.899×10^{-3}	
(-)Q/I	6.456×10^{-3}	
(+)U/I	7.296×10^{-3}	
(-)U/I	4.934×10^{-3}	
(+)V/I	1.269×10^{-3}	
(-)V/I	1.854×10^{-3}	

It delivers an overall efficiency of 1.0. The modulation and demodulation matrices taking into account the polarimeter response matrix, X, of our system are

$$M_{cal,4-image} = \begin{pmatrix} 0.9659 & 0.6183 & 0.5152 & 0.5370 \\ 0.9714 & 0.5822 & -0.5384 & -0.6073 \\ 1.0326 & -0.5621 & -0.6374 & 0.5868 \\ 1.0301 & -0.6384 & 0.6606 & -0.5164 \end{pmatrix},$$
(28)

$$D_{cal,4-image} = \begin{pmatrix} 0.2500 & 0.2500 & 0.2500 & 0.2500 \\ 0.4652 & 0.3918 & -0.3875 & -0.4173 \\ 0.4259 & -0.4088 & -0.4383 & 0.4256 \\ 0.4683 & -0.5087 & 0.4170 & -0.3775 \end{pmatrix}.$$
(29)

Therefore, in our measurements, the polarization efficiencies of Q, U, and V components are 0.6001, 0.5886, and 0.5610, respectively.

Figure 7 shows the measured and calibrated results of the 37 discrete states of the polarization light source for the Q, U, and V, respectively, using this traditional 4-image modulation scheme. Table 7 shows the RMS measurement error for each Stokes component, which characterizes the accuracy of this traditional polarimeter. It can be seen that the polarization accuracy is around the 10^{-3} level, which is about 10 times larger than that of our proposed polarimeter discussed in the previous two subsections. Therefore, the traditional 4-image polarimeter shows lower polarization accuracy under the same test conditions in this experiment.

4.4. Crosstalk Comparison

In this subsection, we will investigate the crosstalk in one polarization component induced by the other components, in the case where the two LCVR retardances are deviated from their theoretical values, with the goal to compare our 6-image polarimeter with the traditional 4-image one. We assume a retardance error of 1/100 working wavelength, for both



109 Page 18 of 23 D. Ren et al.

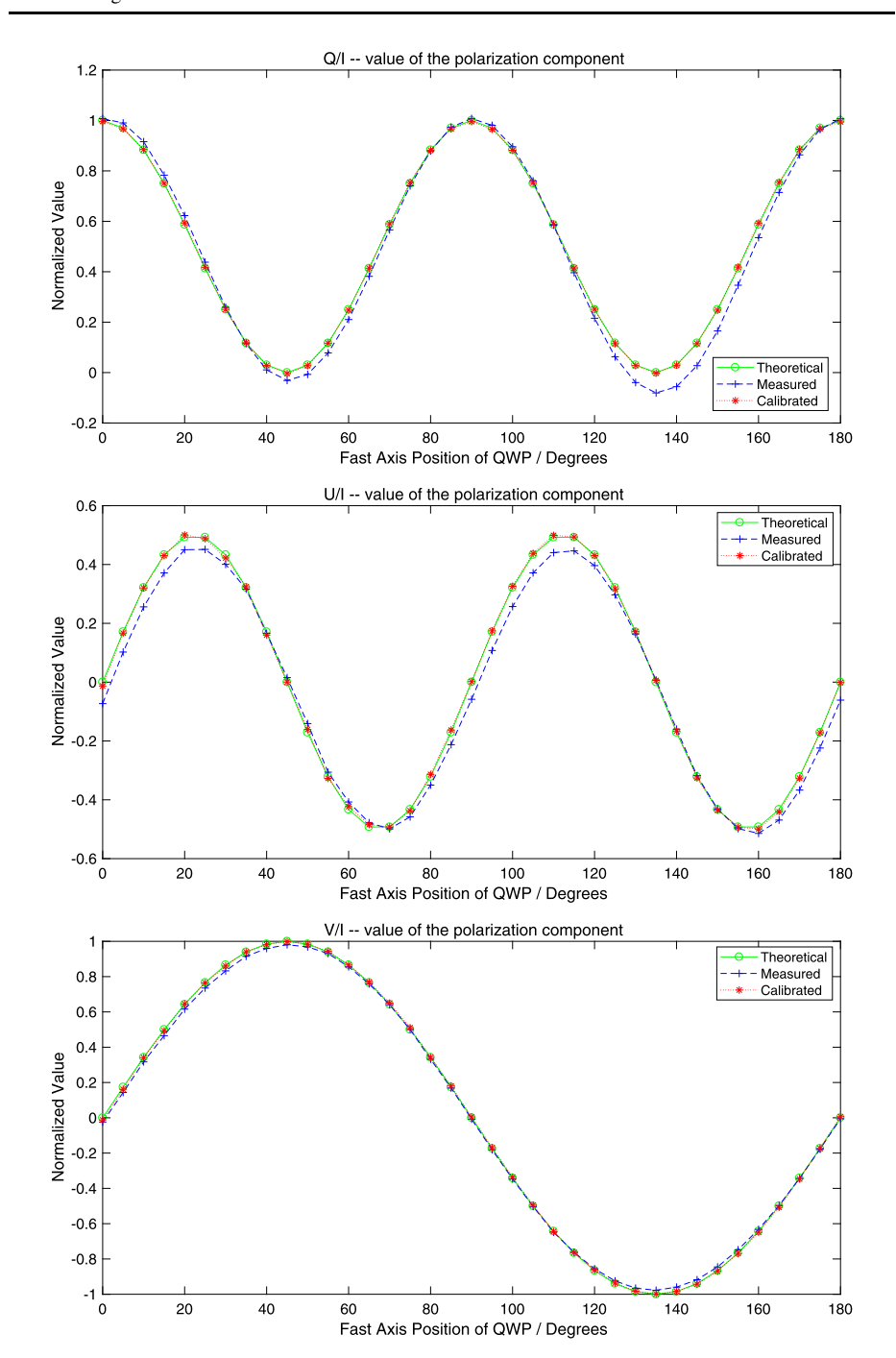


Figure 7 Measured and calibrated results of different generated states of polarized light for the traditional 4-image polarimeter. From top to bottom the normalized Stokes Q, U, and V components, respectively. Green lines represent the theoretical data, blue lines the measured data before the polarization calibration, and red lines the data with polarization calibration.



the Thorlabs LCC1223-A LCVRs used in our polarimeter, even though higher precision may be available for custom-made ones in our future development. We further assume that the first LCVR has a positive retardance error, while the second LCVR has a negative retardance error, since other combinations such as a positive retardance error for both LCVRs will yield a zero value for some of the crosstalk components in one of the polarimeters, which would make the comparison less valid.

Let the $\Delta\delta=\lambda/100$ be the retardance error with a positive value, where λ is the wavelength. The retardance error is added on the LCVR 1 and LCVR 2 as $\phi_1'=\phi_1+\Delta\delta$ and $\phi_2'=\phi_2-\Delta\delta$, respectively. For our proposed 6-image polarimeter, the polarimeter modulation matrix $M_{6-image}'$ can be calculated according to the Mueller matrices from Equation 1, which is

$$M'_{6-image} = \begin{pmatrix} 1 & 0.9998 & -0.0018 & 0.0184 \\ 1 & -0.9998 & 0.0018 & -0.0184 \\ 1 & -0.0018 & 0.9998 & -0.0184 \\ 1 & 0.0018 & -0.9998 & 0.0184 \\ 1 & -0.0184 & -0.0444 & 0.9988 \\ 1 & 0.0184 & 0.0444 & -0.9988 \end{pmatrix}.$$
(30)

With these retardance errors added, we calculate the output Stokes vector with the fully polarized input light $S_{in} = \begin{pmatrix} 1, 1, 0, 0 \end{pmatrix}^T$ with Q/I = 1, using the first and second rows of Equation 30 and Equation 5. This solves the normalized Stokes component Q/I = 0.99983. Thus, the crosstalk from Q to Q is 1.70×10^{-4} . By using the third and fourth rows of Equation 30 and Equation 6, the crosstalk from Q to U is 1.80×10^{-3} . Again, using the fifth and sixth rows of Equation 30 and Equation 7, the crosstalk from Q to V is 1.84×10^{-2} . Similarly, for the input polarized light $S_{in} = \begin{pmatrix} 1, 0, 1, 0 \end{pmatrix}^T$ with U/I = 1, using the third and fourth rows of Equation 30 and Equation 6, we have the crosstalk from U to U being 1.70×10^{-4} . In a similar way, the crosstalk from U to Q is 1.80×10^{-3} and from U to V is 4.44×10^{-2} , respectively. Finally, for the input polarized light $S_{in} = \begin{pmatrix} 1, 0, 0, 1 \end{pmatrix}^T$ with V/I = 1, we have the crosstalk from V to V being 1.15×10^{-3} , and the crosstalks from V to V and from V to V being 1.84×10^{-2} , respectively.

For comparison, we also conduct the error analysis with the traditional 4-image polarimeter, with the same retardance errors added on the LCVR 1 and LCVR 2. In this case, the modulation matrix of the traditional 4-image polarimeter is

$$M'_{4-image} = \begin{pmatrix} 1 & 0.5249 & 0.5629 & 0.6385 \\ 1 & 0.6275 & -0.5149 & -0.5841 \\ 1 & -0.5249 & -0.6385 & 0.5629 \\ 1 & -0.6275 & 0.5841 & -0.5149 \end{pmatrix}.$$
(31)

The results for both polarimeters with a retardance error $\Delta\delta = \lambda/100$ on both LCVR 1 and LCVR 2 are shown in Table 8. We can see that while both polarimeters have similar performances for the crosstalks between different polarization components such as the $U \rightarrow V$, the proposed 6-image polarimeter has a small crosstalk induced by the same polarization component to itself (i.e. a small $Q \rightarrow Q$, $U \rightarrow U$ and $V \rightarrow V$), which is about 10 times smaller than that of the traditional 4-image polarimeter. The small self crosstalk means our polarimeter has the potential to deliver a better measurement accuracy, if other polarization components are very small or suppressed. For example, in our laboratory test and calibration, when we measured the polarization component V, we used a light source that only has the V polarization component as the input, and in this case our 6-image polarimeter delivered a



Table 8 The crosstalks of our 6-image polarimeter and the traditional 4-image polarimeter, at the retardance error $\Delta\delta = \lambda/100$ on both LCVR 1 and LCVR 2.

Crosstalk	Proposed polarimeter	Traditional polarimeter
$Q \rightarrow Q$	1.70×10^{-4}	1.97×10^{-3}
$Q \rightarrow U$	1.80×10^{-3}	8.88×10^{-2}
$Q \rightarrow V$	1.84×10^{-2}	0.00
$U \to Q$	1.80×10^{-3}	4.44×10^{-2}
$U \to U$	1.70×10^{-4}	2.34×10^{-3}
$U \to V$	4.44×10^{-2}	6.28×10^{-2}
$V \rightarrow Q$	1.84×10^{-2}	2.72×10^{-3}
$V \to U$	1.84×10^{-2}	6.11×10^{-2}
$V \rightarrow V$	1.15×10^{-3}	2.88×10^{-2}

measurement accuracy of 1.15×10^{-3} , compared with the 2.88×10^{-2} of the traditional one. We used this approach to test and calibrate the Q, U, and V component on our polarimeter system, as discussed in Section 4.1, which provides high measurement accuracy.

4.5. Discussion

Our polarimeter uses a dedicated modulation strategy, in which only two images can be used to measure one Stokes component (i.e. V). This can be explained on the first order approximation by investigating Equation 23. In an ideal situation of no system error, Equations 23 and 15 will be identical. Therefore, from Equation 15, we can use two images to derive a Stokes component, without crosstalk from the other polarization components. That is, we can use images 5 and 6 to derive the Stokes component V. In the case there is a limited system error, Equation 23 will slightly differ from Equation 15. The difference in each corresponding matrix element between these two matrices is dependent on the alignment accuracy of the polarization elements (and the element retardance tolerances). For a good alignment system, the non-relevant elements that can be rounded off in order to derive the Stokes component V from the two images will approach zero (or have a very small value), which has a negligible impact on the measurement accuracy. For example, if we explore the non-relevant elements (i.e. the elements a_{52} , a_{53} , a_{62} , a_{63} in matrix M_{cal}), they have a value in the range from 10^{-1} to 10^{-2} . This indicates that the crosstalk from other polarization Stokes elements (i.e. Q and U) will be suppressed by a factor of 10^{-1} to 10^{-2} . This will not be a problem, since in real scientific observations, such as the case for the SOLIS project, the other non-measured Stokes components are generally weaker than the measured one. In addition, the maximum polarization efficiency in the 2-image case delivers better signal-to-noise ratio, which effectively promotes a measurement with high accuracy. This explains why we can achieve almost the same measurement accuracy for the V component using two images or six images, since it is fundamentally based on the 2-image modulation case (i.e. ideally, there is no difference between the 2-image, 4-image, and 6-image cases for our polarimeter modulation schemes). Therefore, this explanation for the 2-image case can also be applied to the 4-image case (or the 6-image case) for simultaneous measurement of the Q and U linear components with our polarimeter. For a more sophisticated discussion about polarization calibration and accuracy analysis, we refer to Ichimoto et al. (2008).

In this experiment, all the alignments were conducted by manual adjustments of the angular position for the associated mechanical translation stages, as discussed in Section 3.1. It is worth noting that our polarimeter measurement accuracy can be further improved by exploring better alignment techniques. One promising technique is to use the electronic



servo-control translation stages to replace the current manual adjustment based stages, and use a closed-loop to optimize the matrix M_{cal} defined in Equation 23. For that purpose, we can define a merit function as $J=(a_{13}^2+a_{14}^2+a_{23}^2+a_{24}^2+a_{32}^2+a_{34}^2+a_{42}^2+a_{44}^2+a_{52}^2+a_{53}^2+a_{62}^2+a_{63}^2)$, which is the square sum of all the non-relevant elements. The algorithm works to optimize the translation stage angular positions by minimizing the merit function. That is, the closed-loop optimization will minimize the non-relevant elements in the calibrated modulation matrix M_{cal} . We will report the results of this potential closed-loop based optimization technique in our future publication.

5. Conclusion

We present a high-efficiency and high-accuracy polarimeter for solar weak magnetic field measurements. It consists of two LCVRs and a Wollaston prism as the core optics, and a CU with a fixed linear polarizer and a rotating QWP for the system polarization calibration, and a scientific CMOS camera for image recording. Numerical analysis on the modulation strategy and system calibration are discussed, and related experiments are conducted measuring different polarization signals. Our polarimeter uses a dedicated modulation strategy, in which only one Stokes component can be measured using two intensity images, with other Stokes components having almost no contribution to this measurement, so that maximum polarization efficiency and high accuracy are achievable.

Dedicated alignment and calibration techniques optimized for our polarimeter were developed and discussed. The system accuracy was confirmed by the measurements of polarized signals in our experimental tests. Polarization accuracy on the order of $3-7\times10^{-4}$ was achieved. Our polarimeter is flexible. Depending on the nature of the scientific observations, it can also be used to measure two or three polarization components of the Stokes vector with the same polarization measurement accuracy. When only one or two polarization components are measured, it can deliver even higher polarization efficiency. In summary, our polarimeter has the potential to be used for high-efficiency and high-accuracy polarization measurements for future solar synoptic observations.

Acknowledgements We thank the anonymous referee for detailed and valuable comments on our manuscript, with great patience. D. Ren acknowledges the supports from the National Science Foundation (NSF) under the grants AST-1607921 and AST-1906166.

Disclosure of Potential Conflicts of Interest The authors declare that there are no conflicts of interest.

Publisher's Note Springer Nature remains neutral with regard to jurisdictional claims in published maps and institutional affiliations.

References

Asensio Ramos, A., Collados, M.: 2008, Error propagation in polarimetric demodulation. *Appl. Opt.* 47(14), 2541. DOI. ADS.

Asensio Ramos, A., Trujillo Bueno, J., Landi Degl'Innocenti, E.: 2008, Advanced forward modeling and inversion of Stokes profiles resulting from the joint action of the Hanle and Zeeman effects. Astrophys. J. 683(1), 542. DOI. ADS.

Barrick, G., Benedict, T., Sabin, D.: 2010, Correcting Polarization Crosstalk in the ESPaDOnS Spectro-Polarimeter, SPIE Conf. Ser. 7735, 77354C. DOI. ADS.

Beck, C., Schmidt, W., Kentischer, T., Elmore, D.: 2005, Polarimetric Littrow Spectrograph - instrument calibration and first measurements. Astron. Astrophys. 437(3), 1159. DOI. ADS.



109 Page 22 of 23 D. Ren et al.

Beck, C., Bellot Rubio, L.R., Kentischer, T.J., Tritschler, A., Del Toro Iniesta, J.C.: 2010, Two-dimensional solar spectropolarimetry with the KIS/IAA visible imaging polarimeter. *Astron. Astrophys.* 520, A115. DOI, ADS.

- Bernasconi, P.N., Rust, D.M., Eaton, H.A., Murphy, G.A.: 2000, In: Melugin, R.K., Röser, H.-P. (eds.) Balloon-Borne Telescope for High-Resolution Solar Imaging and Polarimetry, SPIE Conf. Ser. 4014, 214. DOI. ADS.
- Bettonvil, F.C.M., Collados, M., Feller, A., Gelly, B.F., Keller, C.U., Kentischer, T.J., López Ariste, A., Pleier, O., Snik, F., Socas-Navarro, H.: 2010, The Polarization Optics for the European Solar Telescope (EST), *SPIE Conf. Ser.* **7735**, 773561. DOI. ADS.
- Bommier, V., Sahal-Brechot, S., Leroy, J.L.: 1981, Determination of the complete vector magnetic field in solar prominences, using the Hanle effect. Astron. Astrophys. 100(2), 231. ADS.
- Bommier, V., Landi Degl'Innocenti, E., Leroy, J.-L., Sahal-Brechot, S.: 1994, Complete determination of the magnetic field vector and of the electron density in 14 prominences from linear polarization measurements in the HeI D₃ and Hα lines. *Solar Phys.* **154**(2), 231, DOI. ADS.
- Casini, R., de Wijn, A.G., Judge, P.G.: 2012, Analysis of seeing-induced polarization cross-talk and modulation scheme performance. Astrophys. J. 757(1), 45. DOI. ADS.
- Collados, M.: 1999, In: Schmieder, B., Hofmann, A., Staude, J. (eds.) High Resolution Spectropolarimetry and Magnetography, ASP Conf. Ser. 184, 3. ADS.
- del Toro Iniesta, J.C., Collados, M.: 2000, Optimum modulation and demodulation matrices for solar polarimetry. *Appl. Opt.* **39**(10), 1637. DOI. ADS.
- Guo, J., Ren, D.-Q., Liu, C.-C., Zhu, Y.-T., Dou, J.-P., Zhang, X., Beck, C.: 2017, Design and calibration of a high-sensitivity and high-accuracy polarimeter based on liquid crystal variable retarders. *Res. Astron. Astrophys.* 17(1), 8. DOI. ADS.
- Harrington, D.M., Kuhn, J.R., Sennhauser, C., Messersmith, E.J., Thornton, R.J.: 2010, Achromatizing a liquid-crystal spectropolarimeter: retardance vs. Stokes-based calibration of HiVIS. *Publ. Astron. Soc. Pac.* 122(890), 420. DOI. ADS.
- Hofmann, A.: 2007, Polarimetry with GREGOR an ongoing project. Sun Geosph. 2(1), 9. ADS.
- Hofmann, A., Rendtel, J.: 2003, In: Fineschi, S. (ed.) Polarimetry with GREGOR, SPIE Conf. Ser. 4843, 112.
 DOI. ADS.
- Horn, T., Hofmann, A.: 1999, In: Schmieder, B., Hofmann, A., Staude, J. (eds.) Liquid Crystal Imaging Stokes Polarimeter, ASP Conf. Ser. 184, 33. ADS.
- Hou, J., de Wijn, A.G., Tomczyk, S.: 2013, Design and measurement of the Stokes polarimeter for the COSMO K-coronagraph. Astrophys. J. 774(1), 85. DOI. ADS.
- Hough, J.H.: 2005, In: Adamson, A., Aspin, C., Davis, C., Fujiyoshi, T. (eds.) Polarimetry Techniques at Optical and Infrared Wavelengths, *ASP Conf. Ser.* **343**, 3. ADS.
- Ichimoto, K., Lites, B., Elmore, D., Suematsu, Y., Tsuneta, S., Katsukawa, Y., Shimizu, T., Shine, R., Tarbell, T., Title, A., Kiyohara, J., Shinoda, K., Card, G., Lecinski, A., Streander, K., Nakagiri, M., Miyashita, M., Noguchi, M., Hoffmann, C., Cruz, T.: 2008, Polarization calibration of the solar optical telescope onboard Hinode. Solar Phys. 249(2), 233. DOI. ADS.
- Jaeggli, S.A., Lin, H., Mickey, D.L., Kuhn, J.R., Hegwer, S.L., Rimmele, T.R., Penn, M.J.: 2010, FIRS: a new instrument for photospheric and chromospheric studies at the DST. Mem. Soc. Astron. Ital. 81, 763. ADS.
- Keller, C.U., Harvey, J.W., Giampapa, M.S.: 2003, In: Keil, S.L., Avakyan, S.V. (eds.) SOLIS: An Innovative Suite of Synoptic Instruments, SPIE Conf. Ser. 4853, 194. DOI. ADS.
- Leroy, J.L., Bommier, V., Sahal-Brechot, S.: 1983, The magnetic field in the prominences of the polar crown. Solar Phys. 83(1), 135. DOI. ADS.
- Leroy, J.L., Bommier, V., Sahal-Brechot, S.: 1984, New data on the magnetic structure of quiescent prominences. Astron. Astrophys. 131(1), 33. ADS.
- Liu, Z., Xu, J., Gu, B.-Z., Wang, S., You, J.-Q., Shen, L.-X., Lu, R.-W., Jin, Z.-Y., Chen, L.-F., Lou, K., Li, Z., Liu, G.-Q., Xu, Z., Rao, C.-H., Hu, Q.-Q., Li, R.-F., Fu, H.-W., Wang, F., Bao, M.-X., Wu, M.-C., Zhang, B.-R.: 2014, New vacuum solar telescope and observations with high resolution. *Res. Astron. Astrophys.* 14(6), 705. DOI. ADS.
- Martinez Pillet, V., Sanchez Almeida, J.: 1991, A proposal for a low instrumental polarization coude telescope. Astron. Astrophys. 252(2), 861. ADS.
- Martínez Pillet, V., Del Toro Iniesta, J.C., Álvarez-Herrero, A., Domingo, V., Bonet, J.A., González Fernández, L., López Jiménez, A., Pastor, C., Gasent Blesa, J.L., Mellado, P., Piqueras, J., Aparicio, B., Balaguer, M., Ballesteros, E., Belenguer, T., Bellot Rubio, L.R., Berkefeld, T., Collados, M., Deutsch, W., Feller, A., Girela, F., Grauf, B., Heredero, R.L., Herranz, M., Jerónimo, J.M., Laguna, H., Meller, R., Menéndez, M., Morales, R., Orozco Suárez, D., Ramos, G., Reina, M., Ramos, J.L., Rodríguez, P., Sánchez, A., Uribe-Patarroyo, N., Barthol, P., Gandorfer, A., Knoelker, M., Schmidt, W., Solanki, S.K.,



- Vargas Domínguez, S.: 2011, The imaging magnetograph eXperiment (IMaX) for the Sunrise balloon-borne solar observatory. *Solar Phys.* **268**(1), 57. DOI. ADS.
- Parejo, P.G., Álvarez-Herrero, A., Capobianco, G., Fineschi, S.: 2019, Polarimetric performance of a polarization modulator based on liquid crystal variable retarders for wide acceptance angles. J. Astron. Telesc. Instrum. Syst. 5, 034002. DOI. ADS.
- Ravindra, B., Prabhu, K., Elayaveilli Rangarajan, K., Shekar, B., Jagdev, S., Madan Mohan, K., Lancelot, P., Chellappan Thulasidharen, K., Gabriel, F., Selvendran, R.: 2016, Full-disk synoptic observations of the chromosphere using hα telescope at the Kodaikanal observatory. *Res. Astron. Astrophys.* 16(8), 127. DOI. ADS.
- Sen, A.K., Kakati, M.: 1997, Instrumental polarization caused by telescope optics during wide field imaging. Astron. Astrophys. Suppl. 126, 113. DOI. ADS.
- Shih, W.-T., Hsieh, M.-L., Chao, Y.F.: 2014, A Compact in-Situ Ellipsometer Using the Liquid Crystal Variable Retarder, SPIE Conf. Ser. 9200, 920009. DOI. ADS.
- Skumanich, A., Lites, B.W., Martínez Pillet, V., Seagraves, P.: 1997, The calibration of the advanced Stokes polarimeter. Astrophys. J. Suppl. Ser. 110(2), 357. DOI. ADS.
- Socas-Navarro, H., Elmore, D., Pietarila, A., Darnell, A., Lites, B.W., Tomczyk, S., Hegwer, S.: 2006, Spinor: visible and infrared spectro-polarimetry at the National Solar Observatory. Solar Phys. 235(1-2), 55. DOI, ADS.
- Solanki, S.K., Inhester, B., Schüssler, M.: 2006, The solar magnetic field. Rep. Prog. Phys. 69(3), 563. DOI. ADS.
- Tyo, J.S.: 2002, Design of optimal polarimeters: maximization of signal-to-noise ratio and minimization of systematic error. *Appl. Opt.* **41**(4), 619. DOI. ADS.
- Wolfe, J.E., Chipman, R.A.: 2006, Polarimetric characterization of liquid-crystal-on-silicon panels. Appl. Opt. 45(8), 1688. DOI. ADS.
- Wu, S.-T., Efron, U., Hess, L.D.: 1984, Birefringence measurements of liquid crystals. Appl. Opt. 23(21), 3911. DOI. ADS.
- Zangrilli, L., Fineschi, S., Loreggia, D., Gardiol, D., Antonucci, E., Cora, A.: 2003, Imaging Stokes polarimeter based on liquid crystals for the study of the K-solar corona. *Mem. Soc. Astron. Ital.* 74, 528. ADS.
- Zangrilli, L., Fineschi, S., Massone, G., Capobianco, G., Porcu, F., Calcidese, P.: 2006, EKPol: liquid crystal polarimeter for eclipse observations of the K-corona. In: Solar Physics and Solar Eclipses (SPSE 2006), 37. ADS.

